Generation of anomalously energetic suprathermal electrons by an electron beam interacting with a nonuniform plasma

Cite as: Phys. Plasmas **22**, 123510 (2015); https://doi.org/10.1063/1.4937785
Submitted: 31 August 2015 . Accepted: 30 November 2015 . Published Online: 16 December 2015

D. Sydorenko, I. D. Kaganovich, L. Chen, and P. L. G. Ventzek

Generation of anomalously energetic suprathermal electrons by an electron beam interacting with a nonuniform plasma

D. Sydorenko,[1] I. D. Kaganovich,[2] L. Chen,[3] and P. L. G. Ventzek[3]
[1]*University of Alberta, Edmonton, Alberta T6G 2E1, Canada*
[2]*Princeton Plasma Physics Laboratory, Princeton University, Princeton, New Jersey 08543, USA*
[3]*Tokyo Electron America, Austin, Texas 78741, USA*

(Received 31 August 2015; accepted 30 November 2015; published online 16 December 2015)

Generation of anomalously energetic suprathermal electrons was observed in simulation of a high-voltage dc discharge with electron emission from the cathode. An electron beam produced by the emission interacts with the nonuniform plasma in the discharge via a two-stream instability. The energy transfer from the beam to the plasma electrons is ensured by the plasma nonuniformity. The electron beam excites plasma waves whose wavelength and phase speed gradually decrease towards anode. The waves with short wavelength near the anode accelerate plasma bulk electrons to suprathermal energies. The sheath near the anode reflects some of the accelerated electrons back into the plasma. These electrons travel through the plasma, reflect near the cathode, and enter the accelerating area again but with a higher energy than before. Such particles are accelerated to energies much higher than after the first acceleration. This mechanism plays a role in explaining earlier experimental observations of energetic suprathermal electrons in similar discharges. © *2015 AIP Publishing LLC*. [http://dx.doi.org/10.1063/1.4937785]

I. INTRODUCTION

The collisionless relaxation of high-current electron beams and plasma jets is important for many applications: solar disruptions,[1] collective stopping of intense electron beams for inertial fusion applications,[2,3] collisionless shocks and collision of flowing plasmas in astrophysics,[4] and generation of suprathermal electrons (STEs).[5] Such beams are common in laboratory plasmas. Electrons emitted by electrodes surrounding or immersed in the plasma are accelerated by the sheath electric field and become the electron beams penetrating the plasma. In plasma applications where controlling the electron velocity distribution function (EVDF) is crucial,[6] these beams are an important factor capable of modifying the EVDF and affecting the discharge properties.

Recently, Xu *et al.*[7] and Chen and Funk[8] reported an EVDF measured in a dc-rf discharge with 800 V dc voltage which has not only a peak at 800 eV corresponding to the electrons emitted from the dc-biased electrode but also a significant fraction of accelerated electrons with energy up to several hundreds eV. In Refs. 7 and 8, the acceleration is explained invoking nonlinear wave-particle interactions.[9–13] It is suggested that the 800 eV beam excites fast plasma waves which decay parametrically into plasma waves with much shorter wavelength and lower phase velocity and ion acoustic waves, and then the short-wavelength plasma waves accelerate slow electrons of the low-temperature plasma bulk. A similar mechanism may explain enhanced energetic tails in the energy spectrum of electrons in aurora.[14] Other mechanisms invoked to explain the EVDF structure include phase-bunching, kinematic effect of electrons being trapped between rf and dc potentials and released towards the rf electrode during short period of time when the rf voltage is small compared to the dc voltage.[15]

In order to further understand the mechanism of acceleration in the experiment of Refs. 7 and 8, a beam-plasma system was simulated using a 1D3V particle-in-cell code EDIPIC.[16] The EDIPIC was extensively benchmarked against available analytical predictions for two-stream instability in linear and nonlinear regimes. Simulation results discussed below show that the acceleration may be caused not only by the nonlinear effects but by the effects related to the plasma nonuniformity as well. Note that profiling the background plasma density is a method to control the beam energy deposition in plasma.[2,17] In particular, one can excite the instability and achieve beam energy deposition in desirable regions while suppressing the instability in undesirable regions by employing convective stabilization effects.[12,18] In Refs. 19–21 an experimental study and particle-in-cell simulations of interaction of an electron beam with an inhomogeneous, bounded plasma showed formation of localized intense high-frequency fields in density gradient areas.

The present paper discusses the mechanism of generation of suprathermal electrons found in the simulation. In this process, the beam excites plasma waves with long wavelength in the plasma body, these waves are converted into plasma waves with short wavelength at the plasma periphery where the plasma density decreases, and the short-wavelength waves accelerate bulk electrons. Some of these electrons return into the acceleration area again due to reflections from the sheath regions near the plasma boundaries. The second interaction with the short-wavelength plasma waves yields electrons with energies more than 30 times higher than the initial electron bulk temperature. These are the anomalously energetic electrons mentioned in the title of the paper. Repeating the acceleration for the same particle is more efficient than a one-time interaction between particles and plasma waves in density gradient areas considered, e.g., in Ref. 21.

The paper is organized as follows. Section II contains simulation details. Behavior of suprathermal electrons in the simulation and generation of short-wavelength plasma waves is discussed in Section III. Detailed test particle study of electron acceleration is described in Section IV. The results are summarized in Section V.

II. SIMULATION SETUP

The simulated collisionless plasma is bounded between anode (x = 0) and cathode (x = 40 mm). The ion mass is 40 amu which corresponds to argon. In the absence of collisions, particle velocity components parallel to the boundaries are of no importance and the simulation becomes one-dimensional not only in the real space but in the velocity space as well. The grid resolution is 5.877×10^{-6}m, and the time step is 2.335×10^{-13}s. The cathode potential is zero, and the anode potential is $\Phi_A = 800$ V. The cathode can emit electrons with a constant flux and a temperature of 1 eV. The ions are adsorbed at the boundaries. The initial state of the system shown in Fig. 1 is the result of a preliminary simulation which starts with uniform plasma density $n_0 = 2 \times 10^{17}\text{m}^{-3}$, the emission from the cathode turned off, the electron temperature $T_{e,0} = 2$ eV, and the ion temperature $T_{i,0} = 0.03$ eV. The preliminary simulation lasts for 4000 ns. During this time, wide areas with plasma density gradients form as shown in Fig. 1(a). The time counter in the simulations with the beam starts at $t = 0$ and the electron emission starts at $t = 50$ ns. The emission current is 20.13 mA/cm^2, and the relative beam density $\alpha = n_b/n_0$ in the plasma density plateau area (12 mm $< x <$ 27 mm) is $\alpha = 3.77 \times 10^{-4}$. In simulation with the beam, the ion dynamics is included as well. This causes gradual modification of the density profile, in particular the plateau area shrinks. Since the two-stream instability in finite-length plasmas is sensitive to the length of the plasma,[22] this causes significant changes in the instability pattern with time. Such effects are not a subject of the present paper which is why the simulation is stopped at 200 ns before they begin to appear.

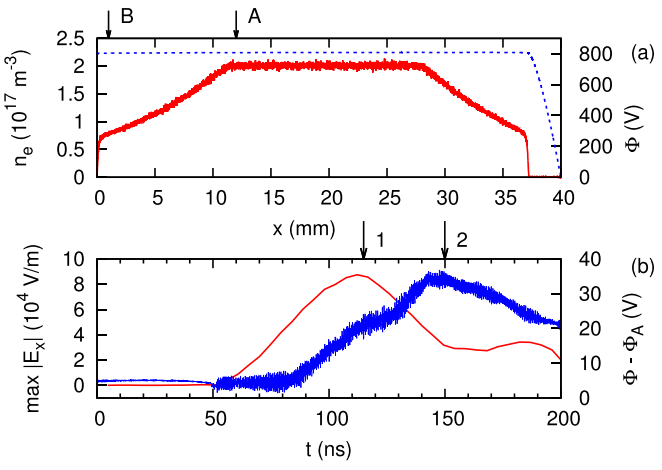

FIG. 1. (a) Profiles of electron density (solid red, left vertical coordinate axis) and electrostatic potential (dashed blue, right vertical coordinate axis) immediately before the electron emission at the cathode begins, $t = 49$ ns. (b) The amplitude of the electric field oscillations vs time (smooth red curve, left vertical coordinate axis) at point $x = 12$ mm (marked by arrow A in (a)) and the plasma potential relative to the anode vs time (blue curve with noise representing plasma oscillations, right vertical coordinate axis) at point $x =$ 1 mm (marked by arrow B in (a)). Arrows 1 and 2 in (b) mark times when snapshots shown in Figures 2 and 3, respectively, are obtained.

The purpose of the selected setup is not to reproduce some specific discharge device but rather to study interaction between an energetic electron beam and a nonuniform plasma of finite length. With plasma ionization by beam electrons turned off, the setup approximates a situation when the beam propagates in a plasma sustained not by the beam but by some other energy source, for example, the rf voltage. Omitting the electron-neutral collisions is reasonable for neutral gas pressures of the order of a few mTorr as discussed below. The time of round travel of suprathermal 20 eV electrons between the walls of a 40 mm system is 3×10^{-8} s, and the same time between collisions (inverse collision frequency) is achieved in an argon plasma for the pressure of 3.6 mTorr. At such a pressure, the effect of plasma bulk scattering on the two-stream instability will be minimal (see the following). The growth rate for the electric field amplitude in Fig. 1(b) is about 10^8 s^{-1}. For 2 eV electrons in an argon plasma, the frequency of elastic electron neutral collisions reaches this value for a rather high neutral gas pressure of about 130 mTorr (the effect of collisions will be described in a separate paper[23]). These estimates are made with cross sections found in Refs. 24 and 25. Finally, for the plasma density and temperature considered in the paper, the electron-ion Coulomb collision frequency[26] is of the order of 2.2×10^6 s^{-1} and therefore also can be omitted.

It is necessary to mention that in the simulation, the density gradients appear in order to maintain continuity of ion flows, while the ions accelerate freely towards the walls. At pressures of about 100 mTorr and higher, the resonance charge exchange collisions between argon ions and neutrals are important,[27] which affects both the ion flow velocity and the density profile. Note that a study of mechanisms of density gradient formation in discharge plasmas is a complex subject by itself and is out of the scope of this paper. For example, in capacitive discharges, similar to the one described in Ref. 7, nonuniformity of the plasma density depends on numerous parameters such as geometry, pressure, applied power, and frequency.[28–31]

III. BEHAVIOR OF SUPRATHERMAL ELECTRONS IN THE SIMULATION

In the density plateau area, the wavelength of the plasma waves excited by the beam is close (but not exactly equal)[22] to $2\pi v_b/\omega_{pe,0}$, where v_b is the electron beam velocity, $\omega_{pe,0} = e(n_0/m_e\varepsilon_0)^{1/2}$, e is the elementary charge, and m_e is the electron mass; the amplitude of the waves grows towards the anode along the direction of beam propagation (see Figs. 2(a) and 3(a)). In the density gradient area, $x < 12$ mm, the profile of the electric field drastically changes: the amplitude and the wavelength decrease towards the anode. Phase plots in Figs. 2(b) and 3(b) show that bulk plasma and beam electrons perform strong oscillations in the electric field of the plasma waves. The EVDF with the STEs near the anode is shown in Fig. 4. They are accelerated from few $T_{e,0}$ up to 65 eV.

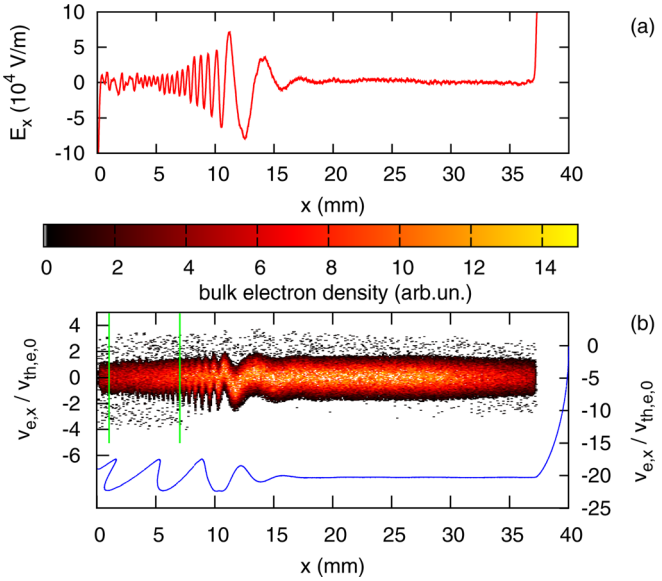

FIG. 2. (a) Profile of the electric field. (b) Phase plane "coordinate-velocity" of bulk electrons (color map, left vertical coordinate axis) and the electron beam (blue, right vertical coordinate axis). In (b), vertical green lines mark range of coordinates of particles used to calculate the velocity distributions in Fig. 4. The snapshots are obtained at time 114.97 ns marked by arrow 1 in Figure 1(b).

The process of acceleration is demonstrated in Figs. 5 and 6 where the color map of the electric field $E_x(x,t)$ is combined with the trajectories of several electrons. The change of the slope of field pattern seen in the color map (Figs. 5(a) and 6(a)) corresponds to the decrease of the phase velocity towards the anode due to the plasma density inhomogeneity. A simple analytical expression estimating the wave phase velocity in the density gradient region can be obtained as follows. The frequency of the wave excited by the beam $\omega = 2.52 \times 10^{10}\,\mathrm{s}^{-1}$ is the same everywhere (within frequency resolution of the calculated spectrum), including the density gradient regions (see the spectrum in

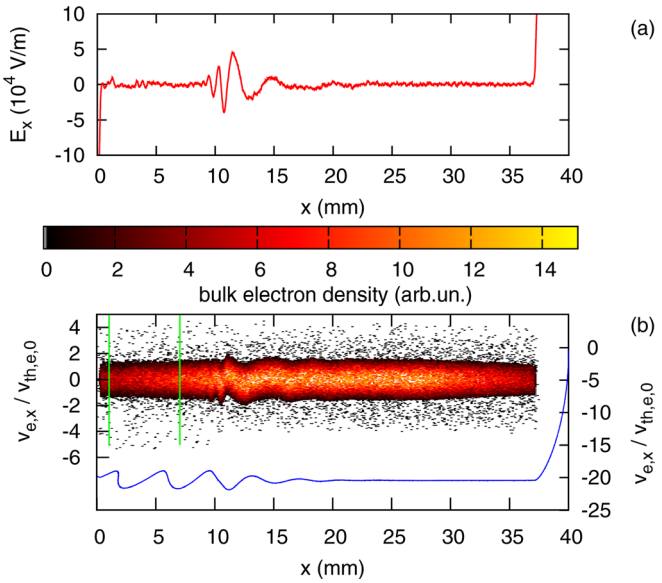

FIG. 3. Same as in Figure 2, but the snapshots are obtained at time 149.96 ns marked by arrow 2 in Figure 1(b).

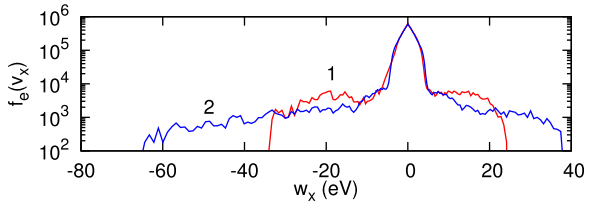

FIG. 4. Bulk electron velocity distribution function obtained using particles with 1 mm $< x <$ 7 mm, the horizontal axis is in energy units, and negative values correspond to propagation in the negative x-direction. Curves 1 (red) and 2 (blue) are for the system states shown in Figures 2 and 3, respectively.

Fig. 7(a)). It is very close to the plasma frequency in the density plateau $\omega_{pe,0} = 2.5214 \times 10^{10}\,\mathrm{s}^{-1}$ (see Fig. 7(b)). Assuming that the dispersion of the plasma wave in the density gradient region is $\omega^2 = \omega_{pe}^2 + 3k^2T_e/m_e$, where T_e is the

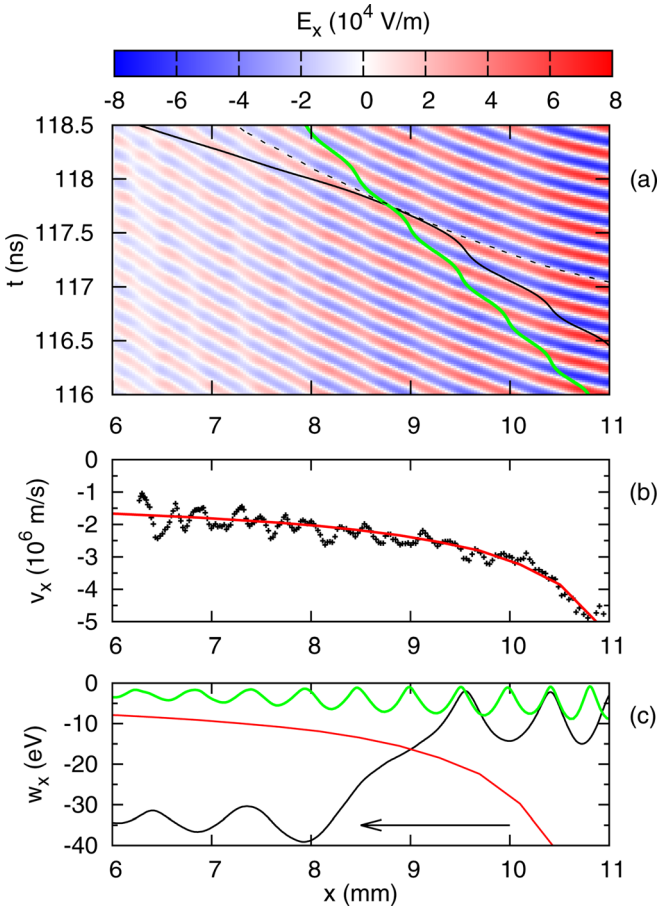

FIG. 5. Interaction of test particles of different initial energies with the waves. (a) Color map of the electric field as a function of coordinate and time $E_x(x,t)$. The positive electric field shown with the red color is directed rightward, towards the cathode. The curves are the test particle trajectories $x(t)$. (b) Wave phase velocity vs coordinate. Here the solid red curve represents Eq. (1), while the black markers correspond to the wave phase velocity calculated from the slope of a zero electric field level line shown by the black dashed curve in (a). (c) Energy of test particles vs coordinate. In (a) and (c), the black solid curves correspond to a particle with initial energy 7 eV at $x = 20$ mm at $t = 110.77$ ns, and the green curves correspond to a particle with initial energy 4 eV at $x = 20$ mm at $t = 108.08$ ns. In (c), the solid red curve is the energy of an electron with the velocity equal to the theoretical local phase velocity of the wave given by Eq. (1). The negative energy values in (c) and the negative velocity values in (b) correspond to propagation in the negative x-direction (towards the anode), and the arrow in (c) points in the direction of propagation of the test particles.

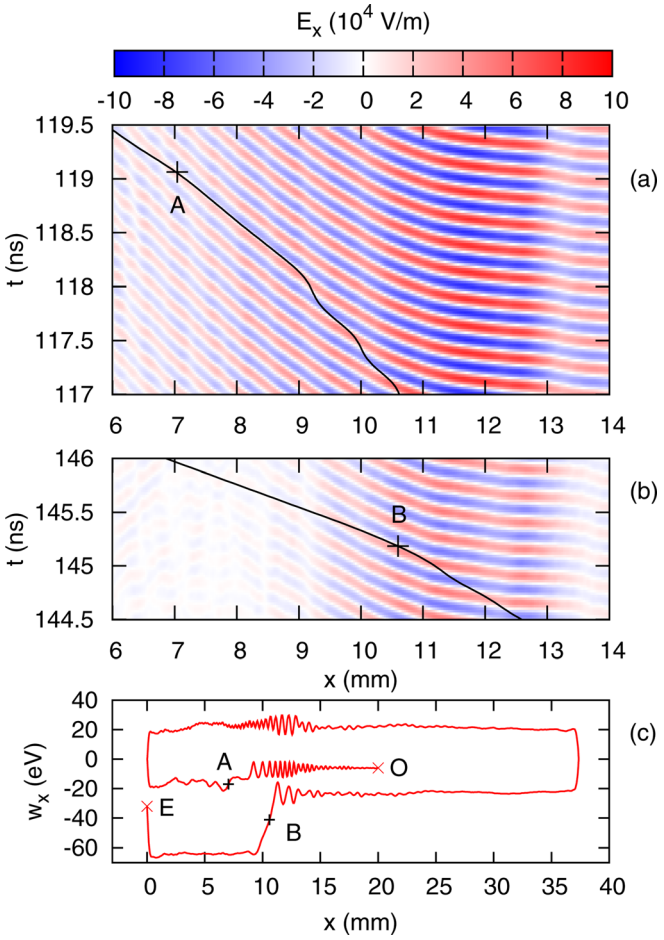

FIG. 6. Two-stage acceleration of a test particle. The initial energy is 6 eV at $x = 20$ mm at $t = 110.44$ ns. (a) The first stage: color map of the electric field as a function of coordinate and time $E_x(x,t)$. The positive electric field shown with the red color is directed rightward, towards cathode. The curve is the test particle trajectory $x(t)$. (b) Same as (a) but for the second stage. (c) Energy of the test particle vs coordinate. In (b), the negative values of energy correspond to propagation in the negative x-direction (towards the anode). Point O marks the starting point, point A—acceleration in the first stage, point B—acceleration in the second stage, and point E—escape of particle at the anode. Note that the deceleration to a complete stop near the walls and the subsequent acceleration in the opposite direction (i.e., the reflection) occur on a distance of about 0.2 mm (anode) and 0.3 mm (cathode).

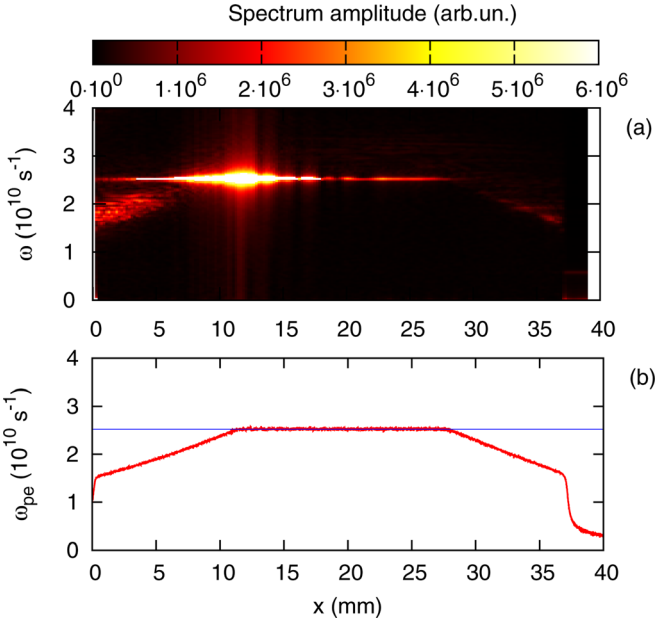

FIG. 7. (a) Amplitude of the frequency spectrum as a function of coordinate and frequency: the spectrum is obtained for the time interval 99 ns $< t <$ 123 ns with $N = 2048$ data points and $\Delta t = 0.01168$ ns time step, and the frequency resolution is $\Delta\omega = 2\pi/N\Delta t = 0.026 \times 10^{10}$ s^{-1}. (b) Profile of the electron plasma frequency obtained at time 114.97 ns marked by arrow 1 in Figure 1(b). The blue line marks the electron plasma frequency $\omega_{pe,0}$ associated with the density plateau in the middle of the plasma.

electron temperature and the wave frequency is $\omega = \omega_{pe,0}$, one obtains $k^2 = (\omega_{pe,0}^2 - \omega_{pe}^2)/(3T_e/m_e)$. With $\omega_{pe}^2 = \omega_{pe,0}^2 n(x)/n_0$, where $n(x)$ is the plasma density depending on coordinate x, the wave phase velocity $v_{ph} \equiv \omega/k = \omega_{pe,0}/k$ becomes the following function of coordinate:

$$v_{ph}(x) = \frac{\sqrt{3T_e/m_e}}{\sqrt{1 - n(x)/n_0}}. \quad (1)$$

The value of (1) becomes infinite as $n(x)$ approaches n_0. A reasonable requirement which prevents application of (1) too close to the plateau is $v_{ph}^2(x) \ll v_b^2$ which transforms to

$$n_0 - n(x) \gg n_0 \frac{3T_e}{2w_b}, \quad (2)$$

where $w_b = m_e v_b^2/2$ is the beam energy. For the density profile, the electron temperature, and the beam energy selected in the paper, criterion (2) allows to use (1) for $x < 11$ mm. In this area, the analytical expression for the phase velocity (1) is in good agreement with the results of the numerical simulation (compare the red curve with the black markers in Fig. 5(b)).

After the emission from the cathode started, STEs moving towards the anode appear first downstream of the area with the strongest oscillations (see Fig. 2(b) for $x < 8$ mm). At the peak of the instability (arrow 1 in Fig. 1(b)), the maximal energy of these electrons reaches about 34 eV (see curve 1 in Fig. 4). While the accelerated electrons escape to the anode, the plasma potential relative to the anode increases (see the blue curve in Fig. 1(b) for 80 ns $< t <$ 150 ns). Some STEs are reflected by the enhanced potential barrier of the anode sheath and, after a round trip through the plasma with another reflection near the cathode, they return into the area with intense plasma oscillations. When it happens, the energies of STEs moving towards the anode downstream of the instability maximum increase even more (see Fig. 3(b) and curve 2 in Fig. 4). The maximal energy of STEs (registered at $t = 139.97$ ns) is about 80 eV. At the first minimum of the electric field amplitude as a function of time (arrow 2 in Fig. 1(b)), the maximal energy is lower, about 65 eV, but still almost twice the maximal energy of the one-stage acceleration (compare curves 2 and 1 in Fig. 4).

IV. TEST PARTICLE STUDY OF ELECTRON ACCELERATION

Acceleration of bulk electrons by waves with short wavelength in the density gradient area is studied with test particles which start in the density plateau area with velocities directed towards the anode. Three particles with initial

energies of 4 eV, 7 eV, and 6 eV representing three different scenarios: no acceleration, one-stage acceleration, and two-stage acceleration, respectively, are discussed below. The 4 eV particle does not get net acceleration, and its energy only oscillates along the trajectory (see the green curves in Fig. 5). The velocity of this particle never reaches v_{ph}.

The 7 eV particle gets significant one-stage acceleration (see the solid black curves in Fig. 5). For $x > 9.5$ mm, this particle is relatively slow and the wave field only causes oscillations of the particle energy with significant amplitude. Near $x = 9$ mm, the particle velocity equals to the local value of v_{ph} (compare the black and the red curves in Fig. 5(c)). The irreversible transfer of energy from the wave to the particle occurs on segment 8 mm $< x <$ 9.5 mm. Note that contrary to well known systems where a particle is gradually accelerated by a wave along the direction of the growth of v_{ph},[32] here the acceleration occurs in the direction of the decrease of v_{ph}. This becomes possible because the wave amplitude rapidly decreases in the same direction, so after the acceleration the particle appears in the area with low field amplitude and cannot be trapped by the wave. The particle becomes a free-flying particle with oscillating energy, but now it is faster than the wave, see the black curve in Fig. 5(c) for $x < 8$ mm. The average energy of the 7 eV test particle after the acceleration is about 34 eV which is sufficient to penetrate through the sheath potential barrier (about 23 eV).

It is necessary to mention that while the fate of the low energy (4 eV) test particles is largely insensitive to the selection of time when these particles are released, the efficiency of acceleration of particles with higher energies does depend on this time and thus the phase of the wave where the test particles are placed. While some of these particles get substantial energy after the first acceleration and escape the plasma, as described in the paragraph above, others acquire lower energy and remain trapped. The selected 6 eV test particle after the first acceleration (point A in Figs. 6(a) and 6(c)) has only 20 eV. This particle is reflected by the anode sheath, travels through the whole plasma, reflects near the cathode, and approaches the instability area with the energy of about 20 eV (see Fig. 6(c)). The particle is accelerated again at the segment between 9.5 mm and 11.5 mm (see point B in Figs. 6(b) and 6(c)). The energy of the particle after the acceleration is about 65 eV, which is more than ten times the initial particle energy. The first acceleration occurs similar to the case described in the previous paragraph except that due to the lower initial particle speed the acceleration occurs closer to the anode where the wave amplitude is lower (compare Figs. 6(a) and 5(a)).

The second acceleration occurs in the area immediately adjacent to the density plateau where the wave phase speed and, in general, amplitude are higher. Note that by this time the short-wavelength waves in the majority of the density slope area decayed because they were involved in intense acceleration of plasma particles (see Figs. 6(b) and 3(a) for $x < 9$ mm), and the instability amplitude is also noticeably lower than during the first acceleration (compare wave fields in Figs. 6(a) and 6(b)). The decay of the plasma waves is a significant limiting factor for the observed two-stage accelerating mechanism.

V. SUMMARY

Summarizing, in a dc plasma-beam system with nonuniform density, suprathermal electrons are generated by short-wavelength plasma waves excited at the density gradients. Some of the accelerated electrons may be reflected by the anode sheath and reintroduced into the two-stream instability area where they will be accelerated one more time. The energy of an electron after the second acceleration can be an order of magnitude higher than its initial energy and few times more than its energy after the first acceleration stage. The simulation above, unlike the experiments of Refs. 7 and 8, does not include the rf voltage. This has both favorable and negative consequences. On one hand, variation of the energy of the beam by the rf voltage may reduce the efficiency of excitation of plasma waves. On the other hand, in a real dc-rf system, plasma bulk electrons are trapped (at least part of the rf period) in a potential well much deeper than the one created by thermal electron motion. This will prevent suprathermal electrons from escaping to the walls and allow them to go through two or more acceleration cycles as described above.

ACKNOWLEDGMENTS

D. Sydorenko and I. D. Kaganovich are supported by the U.S. Department of Energy.

[1]D. B. Melrose, *Instabilities in Space and Laboratory Plasmas* (Cambridge University Press, 1986), Chap. 3 and 4.
[2]V. M. Malkin and N. J. Fisch, Phys. Rev. Lett. **89**, 125004 (2002).
[3]A. J. Kemp, Y. Sentoku, V. Sotnikov, and S. Wilks, Phys. Rev. Lett. **97**, 235001 (2006).
[4]A. Balogh and R. A. Treumann, *Physics of Collisionless Shocks: The Space Plasma Shock Waves*, ISSI Scientific Report Series Vol. 10 (Springer Media Verlag, Berlin-Heidelberg-New York, 2011).
[5]P. H. Yoon, T. Rhee, and C.-M. Ryu, Phys. Rev. Lett. **95**, 215003 (2005).
[6]I. D. Kaganovich, V. I. Demidov, S. F. Adams, and Y. Raitses, Plasma Phys. Controlled Fusion **51**, 124003 (2009).
[7]L. Xu, L. Chen, M. Funk, A. Ranjan, M. Hummel, R. Bravenec, R. Sundararajan, D. J. Economou, and V. M. Donnelly, Appl. Phys. Lett. **93**, 261502 (2008).
[8]L. Chen and M. Funk, in 63rd Annual Gaseous Electronics Conference and 7th International Conference on Reactive Plasmas, Paris, France, 2010.
[9]M. Porkolab and R. P. H. Chang, Rev. Mod. Phys. **50**, 745 (1978).
[10]P. A. Robinson, Rev. Mod. Phys. **69**, 507 (1997).
[11]I. H. Cairns and P. A. Robinson, Phys. Rev. Lett. **82**, 3066 (1999).
[12]Y. P. Golovanov, N. I. Elagin, L. P. Zakatov, A. S. Kingsep, and A. G. Plakhov, Sov. J. Plasma Phys. **3**, 349 (1977).
[13]A. V. Arzhannikov *et al.*, Trans. Fusion Technol. **35**(1T), 112 (1999).
[14]K. Papadopoulos and T. Coffey, J. Geophys. Res. **79**, 674, doi:10.1029/JA079i004p00674 (1974).
[15]A. V. Khrabrov, I. D. Kaganovich, P. L. G. Ventzek, A. Ranjan, and L. Chen, Plasma Sources Sci. Technol. **24**, 054003 (2015).
[16]D. Sydorenko, Ph.D. thesis, University of Saskatchewan, 2006.
[17]V. T. Astrelin *et al.*, Sov. Phys. J. Exp. Theor. Phys. **86**, 489 (1998).
[18]D. D. Ryutov, Sov. Phys. J. Exp. Theor. Phys. **30**, 131 (1970).
[19]H. Gunell, J. P. Verboncoeur, N. Brenning, and S. Torven, Phys. Rev. Lett. **77**, 5059 (1996).
[20]M. D. McFarland and A. Y. Wong, Phys. Rev. Lett. **80**, 5540 (1998).
[21]M. Wendt, T. Klinger, C. Franck, and A. Piel, Phys. Scr. **63**, 62 (2001).
[22]I. D. Kaganovich and D. Sydorenko, "Band structure of the growth rate of the two-stream instability of an electron beam propagating in a bounded plasma," e-print arXiv:1503.04695.
[23]D. Sydorenko, I. D. Kaganovich, P. L. G. Ventzek, and L. Chen, "Effect of collisions on the two-stream instability in a finite length plasma," Phys. Plasmas (unpublished).
[24]M. Hayashi, see http://www.nifs.ac.jp/report/NIFS-DATA-072.pdf for National Institute for Fusion Science.

[25]M. Hayashi, see http://dpc.nifs.ac.jp/IPPJ-AM/IPPJ-AM-19.pdf for Institute of Plasma Physics, Nagoya University.
[26]M. A. Lieberman and A. J. Lichtenberg, *Principles of Plasma Discharges and Materials Processing* (John Wiley & Sons, 2005), Chap. 3.3.
[27]D. Rapp and W. E. Francis, J. Chem. Phys. **37**, 2631 (1962).
[28]X.-Z. Jiang, Y.-X. Liu, S. Yang, W.-Q. Li, Z.-H. Bi, X.-S. Li, and Y.-N. Wang, J. Vac. Sci. Technol., A **29**, 011006 (2011).
[29]V. N. Volynets, A. G. Ushakov, D. Sung, Y. N. Tolmachev, V. G. Pashkovsky, J. B. Lee, T. Y. Kwon, and K. S. Jeong, J. Vac. Sci. Technol., A **26**, 406 (2008).
[30]J. P. Boeuf and L. C. Pitchford, Phys. Rev. E **51**, 1376 (1995).
[31]M. A. Lieberman, J. P. Booth, P. Chabert, J. M. Rax, and M. M. Turner, Plasma Sources Sci. Technol. **11**, 283 (2002).
[32]S. P. Gary, D. Montgomery, and D. W. Swift, J. Geophys. Res. **73**, 7524, doi:10.1029/JA073i023p07524 (1968).